Elastically constrained phase-separation dynamics competing with charge process in $LiFePO_4/FePO_4$ system

Tetsu Ichitsubo,[a*] Kazuya Tokuda,[a] Shunsuke Yagi,[b] Makoto Kawamori,[a]
Tomoya Kawaguchi,[a] Takayuki Doi,[c†] Masatsugu Oishi,[d] Eiichiro Matsubara[a]

[a] *Department of Materials Science and Engineering, Kyoto University, Kyoto 606-8501, Japan*
[b] *Nanoscience and Nanotechnology Research Center, Osaka Prefecture University, Osaka 599-8570, Japan*
[c] *Institute for Materials Chemistry and Engineering, Kyushu University, Kasuga 816-8580, Japan*
[d] *Graduate School of Engineering, Kyoto University, Kyoto 606-8501, Japan*

(Dated: September 18, 2014)

Abstract

By using phase-field computer simulations, we have investigated effects of the coherent strain due to the phase separation in the olivine-type $LiFePO_4$. In this system, the coherent elastic-strain energy due to lattice mismatch between $LiFePO_4$ and $FePO_4$ phases accompanied by insertion and extraction of Li ions is considered to play a crucial role in the phase separation kinetics during the charge/discharge process. The present phase-field micromechanics simulations reveal several significant features of the $LiFePO_4/FePO_4$ system accompanying the coherent strain, such as the retardation of the phase separation, the charge rate dependence, the thermodynamic stability of coherent interfaces between dual phases, etc. Nucleation of the new phase is found to be fundamentally unlikely in terms of the elastic strain energy, except for in the vicinity of the surface of particles, and thus the phase separation would be dominated by the spinodal decomposition process. When the nucleus is present precedently, however, the phase separation can proceed in the mixture mode of the domino cascade and spinodal decomposition processes.

* Email: tichi@mtl.kyoto-u.ac.jp
† Present address: Office of Society-Academia Collaboration for Innovation, Kyoto University, Gokasho, Uji, Kyoto 611-0011, Japan

1. INTRODUCTION

Lithium transition-metal phosphates with an olivine structure[1] have attracted much attention as promising positive-electrode materials for Li batteries. In particular, $LiFePO_4$ shows an acceptably large capacity, although insertion and extraction reactions of Li ions take place at relatively low potentials of 3.42 V vs. Li/Li^+. Yamada et al.[2] clearly showed that there are two solid-solution regions outside both endpoints of the miscibility gap at room temperature, and insertion and extraction reactions of Li ions in $LiFePO_4$ basically undergoes a two-phase equilibrium. Furthermore, it is reported that the miscibility gap shrinks and solid-solution regions extend with reduced size of $LiFePO_4$ particles.[3–5] Especially, Gibot et al.[6] prepared nano-sized $LiFePO_4$ particles of about 40 nm, and demonstrated by X-ray diffraction that insertion and extraction reactions of Li ions proceeded forming a solid solution of Li_xFePO_4 over the almost entire composition range, although the electrode-potential variation still indicated two-phase equilibrium.

On the other hand, recently several works reported that the phase separation kinetics are significantly suppressed or retarded.[7–9] These interesting phenomena are generally believed to be due to the elastic strain due to the lattice mismatch.[5, 10, 11] Also in our previous papers,[12, 13] the strain effects have been discussed for negative electrode materials (Sn, Al etc) in Li batteries, which have shown that the electrode potential (open circuit potential) can be significantly affected by the strain energy. Thus, the arguments on a transformation strain by lithiation and delithiation is gradually becoming frequent. In terms of the elastic strain energy, it is usually considered that the nanoparticles are quite advantageous for the phase separation, because the elastic strain accompanied by the phase separation can be easily released in the vicinity of the particle surface (even without introducing misfit dislocations or mosaicity). Since the surface effects are usually enhanced as the particle size decreases, the phase separation is supposed to be facilitated in such small particles. However, in conflict with this expectation, several recent works have shown that nano-sized particles tend to undergo the single phase reaction, as before.[3–5] Thus, at the present stage, it is not yet clarified how the associated elastic strain affects the phase separation during the charge/discharge processes.

For deep consideration of the $LiFePO_4/FePO_4$ system, we need to take account of the elastic strain due to the lattice mismatch accompanied by the phase separation. A phase-field (or time-dependent Ginzburg-Landau) simulation in combination with the micromechanics theory is powerful tool for analyzing the microstructural evolution on structural phase transformations.[14–16] Recently, for $LiFePO_4$ active materials, there are already several related papers on the non-crystalline phase formation,[17] and simulation for Li distribution in one particle.[18] Especially, the recent trailblazing works using the phase-field simulations by Bai, Cogswell and Bazant[11, 19] have successfully provided with deep understanding of the active material and some indications for a further development. In their paper, the free-energy functional (equation 1 therein) consisting of the chemical free energy based on the Li atoms and electrochemical potential of Li ions was given there, but it is surely complicated to understand straightforwardly the physical meaning of the functional. In general, in the case of the ionic active materials in the battery cells, it is necessary to consider the free energy for the ionic active material under an electrostatic potential. In many works previously reported, the free energy functions based on the electric neutral Li atoms (not Li ions) are frequently used, in most cases, without detailed definition. Actually, there are often confusing cases in that the derivative of the free-energy function gives the chemical

potential of what kind of chemical species (i.e., Li atoms or Li ions?).

In this work, we consider the elastic strain effects on the phase separation kinetics of the $LiFePO_4$ system, on the basis of the phase-field simulation with micromechanics theory[20, 21] and Cahn's spinodal decomposition theory.[22–24] First we describe the basic treatment for the Li atoms in ionic positive electrode materials and intend to clearly show the validity of the free-energy functional[11] for the electrochemical phenomena by the present phase-field simulation with a different treatment focusing on the constant current condition (without considering the value of the overpotential). In our earlier work,[16] we have established and demonstrated the methodology for the phase-field (time-dependent Ginzburg-Landau) simulations with the micromechanical theory for the non-conserved system under an external field. Here we try to address how to calculate the microstructure evolution competing with a gradual change in the overall Li composition (by the charge/discharge process), where the conserved parameter is the Li composition and is changed by charge or discharge process.

Next, on the standpoint of the theoretical simulations, we shall describe several significant features in the phase separation accompanying the coherent strain of the $LiFePO_4/FePO_4$ system, and summarize the strain effect on the active materials in the light of previous experimental results. To date, several models (e.g., core-shell, domino-cascade, spinodal-decomposition models) for the charge/discharge processes have been proposed from the viewpoint of the experimental facts and summarized in the literature.[25] Here, from the viewpoint of the computer simulation, we describe the plausible dynamics mode of the charge/discharge process in the $LiFePO_4/FePO_4$ system. As mentioned above, when the particle size is decreased down to the lower limit (about 40 nm by Gibot et al.[6]), the phase separation tends to be suppressed, but what is addressed/discussed here is the phase-separation dynamics under charge when the particle size is sufficiently above the lower limit. The reason why the $LiFePO_4$ nanoparticles undergo the single-phase reaction (without phase separation) will be described elsewhere.[26]

2. COMPUTING PROCEDURES

2.1. Chemical potential of Li atoms in ionic positive active material

As mentioned above, a similar simulation has already been reported very recently,[11] in which an electrochemical-potential-like free-energy functional for neutral Li atoms was considered, and its functional differential was directly substituted to the overpotential term in the Butler-Volmer equation. It is an interesting trial in terms of the mathematical formulation, but this treatment is rather complicated to be understood in terms of dealing with the neutral Li atoms. Here, in order to show the validity of the free-energy functional, we present a more detailed physical meaning for the electrochemical-potential-like free-energy functional given by the paper.[11]

Active materials for positive electrodes of Li batteries generally consist of Li ions and other ions. Then, it seems difficult to consider the chemical potential of "Li atoms", μ_{Li}, in the ionic active materials. It is, however, inevitably required to know the chemical-potential difference between Li atoms in the Li-metal negative electrode and ones in the positive material, which yields the electromotive force (emf) in Li batteries.

According to its definition, the chemical potential of Li atoms, μ_{Li}, is defined as the Gibbs free-energy difference when one Li atom is inserted/extracted into/from the system under the constant pressure and temperature. Thus, when assuming the electrochemical

equilibrium in the positive electrode, we have formally

$$(\mu^{\mathrm{P}}_{\mathrm{Li^+}} + \Phi^{\mathrm{P}} F_{\mathrm{c}}) + (\mu^{\mathrm{P}}_{\mathrm{e^-}} - \Phi^{\mathrm{P}} F_{\mathrm{c}}) = \mu^{\mathrm{P}}_{\mathrm{Li^+}} + \mu^{\mathrm{P}}_{\mathrm{e^-}} = \mu^{\mathrm{P}}_{\mathrm{Li}}, \tag{1}$$

where $\mu_{\mathrm{e^-}}$ and $\mu_{\mathrm{Li^+}}$ are the chemical potentials of electrons and Li ions in the electrode, respectively, F_{c} the Faraday constant, Φ the electric inner potential (electrostatic potential) and the superscript "P" denotes the "positive" electrode. For example, in the case of discharge, after one Li atom is inserted into the system, the Li atom would be separated to one Li ion and one electron in the ionic active material, and in frequent cases the other ions (e.g., Co^{4+} in $LiCoO_2$, Fe^{3+} in $LiFePO_4$, etc) are reduced by the separated electron.

Even for a Li metal negative ("N") electrode, by considering formally one separated Li ion and one electron, we similarly have

$$(\mu^{\mathrm{N}}_{\mathrm{Li^+}} + \Phi^{\mathrm{N}} F_{\mathrm{c}}) + (\mu^{\mathrm{N}}_{\mathrm{e^-}} - \Phi^{\mathrm{N}} F_{\mathrm{c}}) = \mu^{\mathrm{N}}_{\mathrm{Li^+}} + \mu^{\mathrm{N}}_{\mathrm{e^-}} = \mu^{\mathrm{N}}_{\mathrm{Li}}, \tag{2}$$

where $\mu^{\mathrm{N}}_{\mathrm{Li}}$ equals the chemical potential, μ^{0}_{Li}, of a pure Li metal used for a negative electrode. When we consider emf of Li batteries, we should evaluate the difference in the sum of the electrochemical potentials of electrons and Li ions between positive and negative electrodes. As found from Eqs. (1) and (2), instead of these electrochemical potentials, it is convenient to consider the difference in the chemical potential of neutral Li atoms in the positive and negative electrodes.

The above relations always hold even when the electrostatic potential is applied to the electrodes. Here, as an example, let us consider the case when the electrostatic potential of the positive electrode is set at $\Phi^{\mathrm{P}} = \Phi^{\mathrm{ext}}$. Since, throughout this discussion, we are assuming that the positive electrode shows no dielectric polarization under an applied potential, the total free-energy change of the active material is completely canceled even under an electrostatic potential. Then, what is the driving force of the charge/discharge reactions under the applied potential? The answer is the difference in the electrochemical potential of the Li ions between the electrode and the contacting electrolyte outside of the system; the physical meaning is described below.

When one electron is extracted from the electrode under an external applied potential Φ^{ext}, also one Li ion existing inside the active material under Φ^{ext} must be removed simultaneously into the electrolyte of an electrostatic potential Φ^{E}. When the potential difference is written as $\Delta\Phi^{\mathrm{ext}} = \Phi^{\mathrm{ext}} - \Phi^{\mathrm{E}}$, the difference in the electrochemical potential between the positive electrode and the electrolyte is given by $(\mu^{\mathrm{P}}_{\mathrm{Li^+}} + \Delta\Phi^{\mathrm{ext}} F_{\mathrm{c}}) - \mu^{\mathrm{E}}_{\mathrm{Li^+}}$. Since $\mu^{\mathrm{E}}_{\mathrm{Li^+}} + \Phi^{\mathrm{E}} F_{\mathrm{c}} = \mu^{\mathrm{P}}_{\mathrm{Li^+}} + (\Phi^{\mathrm{E}} + \Delta\Phi^{\mathrm{eq}}) F_{\mathrm{c}}$ in an electrochemical equilibrium state (here, $\Delta\Phi^{\mathrm{eq}} = \Phi^{\mathrm{P}} - \Phi^{\mathrm{E}}$), the electrochemical potential difference of the Li ions at the electrode/electrolyte interface is given by $(\Delta\Phi^{\mathrm{ext}} - \Delta\Phi^{\mathrm{eq}}) F_{\mathrm{c}}$, which is the driving force of the anodic reaction in the positive electrode and, in other words, the work produced by the potentiostat. Namely, for thermodynamic phenomena during charge or discharge under an external electrostatic potential, the above electrochemical potential difference should be taken into account in addition to the conventional chemical potential of Li atoms. Thus, it is shown that the free-energy functional presented by Cogswell and Bazant[11] is valid to consider the microstructural evolution under an external electrostatic potential.

2.2. Free-energy function for a spinodal decomposition system

As shown in the above discussion, after all we have to construct the free-energy function with regard to Li atoms and vacancies after extraction of Li atoms. As suggested by Malik et

al.,[27] the free energies of two phases may not be so simple, but actually several works have successfully explained experimental results on this system by using the free energy of the regular solution type.[28, 29] Since the lattice structures of $LiFePO_4$ and $FePO_4$ phases are both orthorhombic and there are just small differences between their lattice constants when their space group falls into $Pnma$, as a first approximation, it is reasonable to assume the free-energy function, $f(\phi)$, of regular solution type for the spinodal-decomposition system. Then, the coarse-grained molar free-energy, $f(\phi)$, is assumed to have the form of the regular solution type:

$$f(\phi) = \Omega\phi(1-\phi) + RT\big[\phi\ln\phi + (1-\phi)\ln(1-\phi)\big], \tag{3}$$

where ϕ is defined as $\phi = 1 - c_{\mathrm{Li}}$ with c_{Li} the Li composition in the lithium site of the olivine structure [i.e., ϕ is the Li-vacancy (denoted as V_{Li}) composition], Ω the regular solution parameter, R the gas constant, and T the temperature; the coarse-grained order parameter ϕ is in the range of $0 \leq \phi \leq 1$. For $\phi = 0$, the order parameter ϕ represents $LiFePO_4$, while it denotes $FePO_4$ for $\phi = 1$. According to the literatures,[11, 17] the value of Ω is about 12 kJ/mol for the $LiFePO_4/FePO_4$ system. When converting to the free-energy density function per unit volume, Eq. (3) has to be divided by the molar volume $V_{\mathrm{m}} \approx 43.8 \times 10^{-6}$ m^3/mol.

Here, μ_{LFP} and μ_{FP} are defined as the chemical potentials of $LiFePO_4$ and $FePO_4$ in the mixture material, $Li_{1-\phi}FePO_4 = (1-\phi)LiFePO_4 + \phi FePO_4$, measured from the chemical potentials of pure $LiFePO_4$ and $FePO_4$, respectively. As is clearly illustrated in Fig. 1(a), the first derivative of molar free-energy function, $f(\phi)$, with regard to ϕ gives

$$\frac{\partial f(\phi)}{\partial \phi} = \frac{\mu_{\mathrm{FP}} - \mu_{\mathrm{LFP}}}{1-0} = -\mu_{\mathrm{Li}}, \tag{4}$$

because we can regard that $LiFePO_4 = FePO_4 + Li$, and then the relation, $\mu_{\mathrm{LFP}} = \mu_{\mathrm{FP}} + \mu_{\mathrm{Li}}$, holds in equilibrium.

Figure 1(b) (lower) shows the free-energy density function per unit volume. Since the chemical potentials of pure $LiFePO_4$ and $FePO_4$ are set to be equal for simplicity (i.e., ${\mu_{\mathrm{LFP}}}^0 = {\mu_{\mathrm{FP}}}^0$), when the system is in the two-phase equilibrium, μ_{Li} equals zero based on Eq. (4). Since emf is experimentally about 3.42 V in the two-phase equilibrium, i.e., $emf = -(\mu_{\mathrm{Li}} - \mu^0_{\mathrm{Li}})/F_{\mathrm{c}} = 3.42$ V, it should be noted that the chemical potential of pure Li metal, μ^0_{Li}, is set at $3.42F_{\mathrm{c}}$. Thus, emf is given by $emf = -\mu_{\mathrm{Li}}/F_{\mathrm{c}} + 3.42$, depicted in Fig. 1(b) (upper).

2.3. Electrochemical delithiation/lithiation process

Let us first begin with the Butler-Volmer equation:

$$j = j_{\mathrm{a}} - j_{\mathrm{c}} = j_0\Big[\exp\big(\frac{(1-\beta)zF_{\mathrm{c}}\eta}{RT}\big) - \exp\big(-\frac{\beta z F_{\mathrm{c}}\eta}{RT}\big)\Big], \tag{5}$$

where j is the total current density, j_{a} and j_{c} the anodic and cathodic current densities, respectively, j_0 the exchange current density, β the symmetry factor, z the valence, and η ($\equiv \Delta\Phi^{\mathrm{ext}} - \Delta\Phi^{\mathrm{eq}}$) the overpotential, which is the difference in the electrode/electrolyte potential differences between with an applied external potential and without the potential. In general, the chemical potential change of Li atoms due to the phase separation causes the change in $\Delta\Phi^{\mathrm{eq}}$, which would affect the strength of the overpotential η at each position

in the electrode, but we here focus on the constant current conditions and the evaluation of the overpotential is out of scope.

Taking account that the current in this case is a vector quantity and the magnitude of $\mathbf{j}_0(\mathbf{x})$ is proportional to the Li composition $c_{\mathrm{Li}}(\mathbf{x})$, Eq. (5) for the each position $\mathbf{x}$ is simplified as

$$\mathbf{j}(\mathbf{x}) \approx k_1\big(1-\phi(\mathbf{x})\big)\bar{\mathbf{j}}(\mathbf{x}), \tag{6}$$

where k_1 is a constant and $\bar{\mathbf{j}}(\mathbf{x})$ is the unit vector of $\mathbf{j}(\mathbf{x})$. Based on the diffusion equation $\partial\phi(\mathbf{x})/\partial t = -\partial c_{\mathrm{Li}}(\mathbf{x})/\partial t = (1/zF_{\mathrm{c}})\nabla\cdot\mathbf{j}(\mathbf{x})$ and a constant current condition, i.e., $J = \int_S \mathbf{j}(\mathbf{x})\cdot\mathbf{n}dS = \int_V \nabla\cdot\mathbf{j}(\mathbf{x})d\mathbf{x} = Const.$ ($\mathbf{n}$ is the unit outer normal vector in the surface element dS), we have a following equation

$$\begin{aligned}\frac{\partial\overline{\phi}}{\partial t} &= \frac{1}{zF_{\mathrm{c}}V}\int_V \nabla\cdot\mathbf{j}(\mathbf{x})d\mathbf{x} \\ &= \frac{k_1}{zF_{\mathrm{c}}V}\int\big(1-\phi(\mathbf{x})\big)\nabla\cdot\bar{\mathbf{j}}(\mathbf{x})d\mathbf{x} = Const.,\end{aligned} \tag{7}$$

where $\overline{\phi}$ is the spatial average of $\phi(\mathbf{x})$, which is given by $\overline{\phi} = (1/V)\int_V \phi(\mathbf{x})d\mathbf{x}$, and V is the volume of the system. After all, Eq. (7) simply means that the delithiation/lithiation amount at each position $\mathbf{x}$ in the charge/discharge process under a constant current condition should be proportional to $1-\phi(\mathbf{x})$.

2.4. Generalized Langevin equation

The kinetic process under a given $\overline{\phi}$ is assumed to be governed by the following Langevin equation,

$$\frac{\partial\phi(\mathbf{x},t)}{\partial t} = L\nabla^2\frac{\delta F\{\phi\}}{\delta\phi} + \theta(\mathbf{x},t), \tag{8}$$

where L is the relaxation rate (assumed to be constant independent of the Li composition) and $\theta(\mathbf{x},t)$ is the thermal fluctuation at a position $\mathbf{x}$ and time t. Since the free-energy consists of the chemical energy and the elastic energy, the free-energy functional $F\{\phi\}$ is given by

$$F\{\phi\} = \int d\mathbf{x}\Big[f\left(\phi(\mathbf{x})\right) + K_{\mathrm{S}}\left|\nabla\phi(\mathbf{x})\right|^2 + f_{\mathrm{el}}\left(\phi(\mathbf{x})\right)\Big], \tag{9}$$

where K_{S} is the gradient coefficient, and the elastic strain energy function f_{el} is given by[20]

$$f_{\mathrm{el}} = \frac{1}{2}C_{pqmn}\big[\varepsilon^*_{pq}(\phi(\mathbf{x})) - \gamma_{pq}(\phi(\mathbf{x}))\big]\varepsilon^*_{mn}(\phi(\mathbf{x})), \tag{10}$$

where C_{pqmn} are the elastic constants, $\gamma_{pq}(\phi(\mathbf{x}))$ is the constrained strain, $\varepsilon^*_{pq}(\phi(\mathbf{x}))$ is the eigenstrain.

In the elastic equilibrium, the total strain $\gamma_{ik}(\mathbf{x})$ is given by[14, 21]

$$\gamma_{ik}(\mathbf{x}) = \sum_{\boldsymbol{\xi}\ \mathrm{space}} C_{jlmn}\overline{\xi}_l A_{ikj}\hat{\varepsilon}^*_{mn}(\boldsymbol{\xi})\exp(i\frac{2\pi}{M}\boldsymbol{\xi}\cdot\mathbf{x}), \tag{11}$$

where $A_{ikj} = (G_{ij}^{-1}\overline{\xi}_k + G_{kj}^{-1}\overline{\xi}_i)/2$ with $G_{ij} = C_{ipjq}\overline{\xi}_p\overline{\xi}_q$, $\overline{\boldsymbol{\xi}}$ is the unit vector of $\boldsymbol{\xi}$, M the division number of the system for the discrete Fourier transformation, and $\hat{\varepsilon}^*_{mn}(\boldsymbol{\xi})$ the Fourier transformation of $\varepsilon^*_{mn}(\mathbf{x}')$. Especially, if we deal with a special case that one ellipsoidal inclusion is formed in the matrix, on the basis of the Eshelby theory[20], the total strain is given by $\gamma_{ik}(\mathbf{x}) = S_{ikmn}\varepsilon^*_{mn}$, where S_{ikmn} is called the Eshelby tensor; see, for detail, literature[21].

Given that the eigenstrain is given by a linear form of $\varepsilon^*_{mn} = T^*_{mn}\phi$, the partial differential of the strain energy function $f_{\rm el}$ with regard to ϕ is given by

$$\frac{\partial f_{\rm el}}{\partial \phi} = \frac{\partial f_{\rm el}}{\partial \varepsilon^*_{mn}} \cdot \frac{\partial \varepsilon^*_{mn}}{\partial \phi} = -\sigma_{mn} T^*_{mn}, \tag{12}$$

where $\sigma_{mn} = C_{pqmn}(\varepsilon^*_{pq} - \gamma_{pq})$, and T^*_{mn} represents the strength of the eigenstrain. By using the Euler-Lagrange equation for the variation $\delta F/\delta\phi$, the generalized Langevin equation (8) is reduced to

$$\begin{aligned} \frac{\partial \phi}{\partial t} &= L\nabla^2\Big[\frac{\partial f}{\partial \phi} - \sigma_{mn}T^*_{mn} - 2K_{\rm S}\nabla^2\phi\Big] + \theta \\ &\equiv L\nabla^2(-\mu^{\rm total}_{\rm Li}) + \theta, \end{aligned} \tag{13}$$

where $\mu^{\rm total}_{\rm Li}$ denotes the "total" chemical potential of Li atoms consisting not only of the pure thermodynamic chemical potential given by Eq. (4) but also of the elastic-energy and gradient-energy terms. Differently from the treatment of the kinetic equation given by the previous work,[11] the two equations of generalized Langevin equation and charge/discharge kinetic equation are solved simultaneously in this work.

2.5. Parameters and procedure

In the actual simulation, we first execute the charge (discharge) process given by Eq. (7) and subsequently solve Eq. (13). The latter equation has been solved numerically by the Euler technique:

$$\phi(t+\Delta t) = \phi(t) - L\Delta t\nabla^2\mu^{\rm total}_{\rm Li} + \int_t^{t+\Delta t}\theta dt'. \tag{14}$$

The time step and the relaxation rate are set at $\Delta t = 1$ s' (s' is a time unit for the simulation) and $L = 25\times10^{-30}$ m^5/Js', respectively. The thermal noise, $\int_t^{t+\Delta t}\theta dt'$, is given by the Gaussian random number with a zero average and the variance ${s_\theta}^2$, but there exists some difficulty in evaluating it *a priori*; thus, a small value ($s_\theta = 0.005$) is used arbitrarily for the Gaussian random number in the simulations.

We assume that the Li-composition dependence of lattice constants obeys the Vegard law; the magnitude of the eigenstrain is expressed by the order parameter ϕ. Then, the eigenstrain, $\varepsilon^*_{mn}(\phi)$, is measured from the lattice constants of $LiFePO_4$ and given by

$$\varepsilon^*_{mn} = T^*_{mn}\phi = \begin{pmatrix} -0.050 & 0 & 0 \\ 0 & -0.036 & 0 \\ 0 & 0 & 0.019 \end{pmatrix}\phi. \tag{15}$$

In the calculation of the strain energy, eq. (11) has been calculated by the fast Fourier transformation technique. Thereby, a periodic boundary condition is inevitably imposed into the present simulations. The elastic constants of $LiFePO_4$ and $FePO_4$ are assumed to be the same, and the average of both phases obtained by the first-principle calculations (GGA + U)[30] is used for this simulation. The present simulations have been conducted in a two dimensional (2D) system to reduce the computing time; the system is divided into 128×128 areas [i.e. $M = 128$ in eq. (11)], and the divided grid distance is set at $\Delta d = 0.5$ nm. This 2D system assumes that the diffusion of Li atoms (ions) along the b axis is quite fast and the distribution of the Li composition or Li vacancy composition, i.e., the chemical potential of Li atoms, is homogeneous along the b axis.

The gradient coefficients are estimated as follows. When we consider only the free-energy increase due to an one-dimensional interface of the gradient term, we have $\delta F = \int_V K_{\rm S}(d\phi/dx)^2 dxdydz = S\int K_{\rm S}(d\phi/dx)^2 dx \approx SK_{\rm S}\Delta\phi^2/\zeta \equiv \gamma S$, and then we obtain $\gamma = K_{\rm S}\Delta\phi^2/\zeta$, where ζ is the thickness of the interfacial wall, $\Delta\phi$ is the order-parameter difference, which equals $\Delta\phi = 1-2\phi$. On the other hand, according to Cahn-Hilliard theory,[22] the equilibrium-interface thickness is given by $\zeta_e = \Delta\phi_e\sqrt{K_{\rm S}/\Delta f_{\rm max}}$, where $\Delta f_{\rm max}$ is the free-energy difference between at $\phi = 0.5$ and at $\phi = \phi_{\rm e}$ (equilibrium order parameter), $\Delta\phi_{\rm e}$ is the equilibrium order-parameter difference, and $\Delta\phi_{\rm e} \approx 1$ in this case. After all, we obtain a relation

$$K_{\rm S} \approx \frac{\gamma_{\rm e}^2}{\Delta f_{\rm max}}. \tag{16}$$

3. RESULTS AND DISCUSSIONS

3.1. Nucleation process

Before the dynamic simulation, we first show a stable shape and direction of an infinitesimal $FePO_4$ ($LiFePO_4$) precipitate when it is formed in the infinite homogeneous $LiFePO_4$ ($FePO_4$) matrix. Figures 2(a) and 2(b) show the [001] pole figures showing the precipitate-direction dependence of the elastic strain energy $E_{\rm s}$ (a) for the disc-like (plate-like) precipitate and (b) for the rod-like (needle-like) one. These figures indicate that disc-like (or plate-like) shape whose normal axis is along the [101] direction in the reciprocal space is most favorable in terms of strain energy, and disc inclusions whose normal axis is along the [100] direction (i.e., so-called ac plane, frequently observed experimentally) would be also favored (as to the interface stability, we will discussed in a later section). The minimum value of $E_{\rm s}$ amounts to about 100 MJ/m^3, while the driving force of the nucleation $\Delta f_{\rm chem}$ is about $-$80-90 MJ/m^3 in Fig. 1(b), that is, $\Delta f_{\rm chem} + E_{\rm s} > 0$. Incidentally, the strain energy amount to be about 160 MJ/m^3 for the sphere precipitate, and about 130 MJ/m^3 for the rod-like precipitate. Consequently, this hinders the nucleation of $FePO_4$ in the $LiFePO_4$ matrix on charge, and vice versa.

In order to confirm this, the phase-field simulation is performed at $\phi = 0.1$, at which nucleation process is supposed to occur. Figures 2(c) and 2(d) show the changes in the free energy and elastic energy as a function of time (c) with or (d) without the coherent strain due to the lattice mismatch. The simulations also show that the phase separation is difficult to take place via nucleation process when the coherent misfit strain is present. However, the phase separation via nucleation and growth process can easily occur if the coherent strain is absent, despite that the other conditions are totally the same with each

other. Thus, nucleation in this system is basically unlikely to occur in the inner side of the active materials, if any, nucleation can take place only near the surface where the elastic strain would be released relatively easily.

3.2. Spinodal decomposition

On the basis of the above arguments, the b axis (the [010] direction) should be normal to the objective plane to be observed in the 2D simulation, in terms of the diffusion direction[31] and elastic energy. Figure 3(a) (upper) shows the Li composition, free energy, and elastic energy maps in a later stage of the kinetics (t = 20000 s'), which is the microstructure evolution of the phase separation kinetics from the homogeneous matrix of $\phi = 0.5$, being consistent with the above strain energy calculation with the micromechanics theory.This microstructure is also in good agreement with the microstructure pattern by Cogswell et al.,[11] and also very similar to the actual microstructure observed in a transmission electron microscope (TEM)[29, 32, 33]. The modulation length on the separation is about 10-20 nm in this calculation, which means that the gradient energy corresponding to the interfacial energy of 40 mJ/m^2 used in this simulation is judged to be valid.

It is worthwhile to note that there is a certain amount of interface regions with $\phi \sim 0.5$ between the $LiFePO_4$ and $FePO_4$ phases, whose free energy is about 29 MJ/m^3 and elastic energy is almost zero. Namely, the interface regions are not strained when the volume fraction is almost the same as each other. The reason why such non-equilibrium regions are stably present despite that they are unfavorable in terms of the chemical free energy is that the whole strain energy can be considerably reduced, leading to the gain of the total free energy. Consequently, the interface is not a direct attachment of the two phases but consists of a certain interlayer of middle-range composition of Li atoms. This theoretical finding is quite significant in considering the reason why such non-equilibrium regions are frequently observed experimentally.[33]

As seen in Fig. 3(b) (lower), it is also noted that a certain incubation time is needed as well as nucleation process even when the phase separation proceeds via the spinodal-decomposition mode. This phenomenon is caused by the facts that all the spinodal waves cannot be allowed to grow and a certain favorable spinodal-wave direction ([100] or [101] in this case) is present in the system whose elasticity and eigenstrain is strongly anisotropic. For this reason, it looks like a nucleation process even though the spinodal decomposition takes place. Hence, based on this fact, one should not use the Johnson-Mehl-Avrami equation that is available for the nucleation mode for analyzing the phase separation kinetics.

3.3. Strong anisotropic stability of interface between $LiFePO_4$ and $FePO_4$

Next the stability of anisotropic interfaces is discussed. It is frequently reported that the *bc* interface (or *bc* plane) is observed experimentally. Here we show the thermodynamic and mechanical stability of the anisotropic interfaces of (a) the *bc* interface and (b) the *ab* interface; the time evolution of the interfaces after the respective interfaces are set initially as shown in Fig. 4. Obviously, the *bc* interface is found to be stable with the elapse time. On the contrary, the *ab* interface is quite unstable and cannot be retained, tends to collapse with time, being in consistent with the experimental fact that the *bc* interface is frequently observed in the actual TEM observations.[29, 32, 33]

The difference between the interface stabilities is due mainly to anisotropy of the lattice mismatch, which is given by eq. (15). Namely, to understand why the *bc* interface is the most stable, it is significant to notice that the fact that the lattice mismatch along the *a* axis is maximum and that along the *c* axis is minimum in this system, that is, the coherent interface that includes the maximum lattice mismatch along the *a* axis becomes more unstable than the *bc* interface that is not relevant to the *a* axis. From this viewpoint, the *ac* interface is also unfavorable in terms of the elastic strain energy as well. Thus, there is a strong anisotropic stability in the formation of interfaces, so that the core-shell model is unlikely to be realized during charge/discharge process. This fact is quite significant in discussing the dynamics of phase separation by the charge or discharge process.

3.4. Microstructure evolution in charge process

In the case where nucleus is absent in the initial matrix

We show the charge process competing with the phase separation from almost homogeneous $LiFePO_4$ matrix without any initial nuclei. In the light of Fig. 3(a), as the spinodal decomposition almost ends at $t = 20000$ s', we have performed the charge simulations around the C rate of 1/(20000 s'). Figures 5(a) and 5(b) show the kinetics and microstructural evolution during charge (i.e., delithiation) process: (a) C rate $\approx$ 1/(20000 s') and (b) C rate $\approx$ 1/(100000 s'). Thus, also in the charge process, nucleation cannot be observed and, furthermore, the spinodal decomposition is considerably suppressed; the spinodal decomposition does not take place immediately even when the overall Li composition reaches the spinodal point ϕ_s, that satisfies $f'' = \partial^2 f/\partial\phi^2 = 0$ in the phase diagram. When the C rate is lower, the composition at which the spinodal decomposition starts to occur is found to be lower (incidentally the single-phase reaction occurs when the charge rate is quite fast), and thus the phase separation kinetics tends to follow the electrochemical delithiation process. However, even if the C rate is further decreased, it is shown that the nucleation process is absent as seen in Fig. 5(d). Incidentally, in contrast to the former cases, the nucleation can be clearly observed without any lattice mismatch as shown in Fig. 5(c), despite that the C rate is the same as in Fig. 5(b). These results are consistent with Fig. 2 obtained by the argument based on the statics. Again it can be said that it is quite unlikely for the nucleation process to take place inside this active material, and suppression of the phase separation is revealed to be essential in this phase-separation system. Thus, it is demonstrated that the increase of the strain energy due to lattice mismatch conclusively affects its kinetics.

In the case where nucleus is present in the initial matrix

Finally we argue the case where one plate-like $FePO_4$ precipitate exists precedently in the middle of the system. This would correspond to consideration of the case where the nucleation preempts the spinodal decomposition; the nucleation would be possible around the sample surface where the elastic strain would be easily released.

Figure 6 shows the charge (delithiation) process. In this case, the domain wall motion of $LiFePO_4/FePO_4$ like domino cascade precedes spinodal decomposition in the early stage, until the Li composition of the other region reaches spinodal point. In this simulation, such a domino-cascade-like domain motion occurs within the range of around 20 nm in the early

charge stage, followed by the spinodal decomposition in the far distant region from the initial plate, after the system reaches to the spinodal point. Since the initial $FePO_4$ plate is along the (100) plane (this direction is shown to be stable; see Fig. 4), the spinodal wave in the [100] direction is also stable due to the elastic interaction effect. Although the presence of the disordered regions of $\phi \sim 0.5$ plays a significant role for the redox reactions in the domino cascade model reported by Delmas et al.,[34] this simulation can also reproduce the domino cascade behavior even for a simple kinetic model based on the first chemical reaction equation without assuming a specific polaron property in the disordered region of $\phi \sim 0.5$.

It is interesting to note that the interface along the (100) plane in the domino cascade model is elastically stable also in the case of spinodal decomposition and it induces the spinodal wave in the [100] direction. Thus, we can point out that the mixture mode of domino cascade and spinodal decomposition during charge/discharge process is possible in principle, when the particles are sufficiently larger than the lower limit (about 40 nm), especially for nanoparticles of appropriate size where the strain energy due to nucleation is relatively easily released. After the phase separation, probably the many-particle effects[28] play a very significant role in the redistribution of Li ions in respective particles.[35]

4. CONCLUSIONS

We have conducted the computer simulation study to reveal the effects of the lattice mismatch due to the phase separation of olivine $LiFePO_4$. The salient results can be summarized as follows:

1. The definition and physical meaning of the chemical potential of Li atoms in the ionic active materials have been clearly given here, and the driving force of the anodic reaction during a charge process is shown to be given by the difference in the electrochemical potential of Li atoms between the electrode and electrolyte. Thus, the seemingly complicated free-energy functional presented by the previous paper[11] is definitely validated by the present argument. In addition, the charge process under the cc condition has been analyzed by solving the simultaneous equations of the first-order reaction equation (7) and generalized Langevin equation (13). We have substantiated that both of the simulation procedure presented here and Butler-Volmer kinetics presented in the paper[11] are validated for the simulation of the electrochemical phenomena of the storage batteries.

2. Our phase-field simulations revealed that the nucleation is unlikely when the lattice mismatch is present while it is possible without the lattice mismatch. This is different from the previous result by the simulations[11], which would be caused by the difference in whether the relaxation near the surface is taken into account or not. Thus, in terms of the elastic energy, as shown in Fig. 2, the nucleation of new phase during charge or discharge process is unlikely to take place inside the particles, and fundamentally it would be only possible near the particle surface. Therefore, on the charge/discharge processes, the system needs to wait for the composition region where the spinodal decomposition can take place. However, in the light of the experimental facts that reducing the particle size tends to cause the solid-solution reaction (without phase separation),[3–6] the phase separation by nucleation seems to be fundamentally quite difficult to occur in this system, being consistent with the present simulation results.

3. Even though the overall composition is within the composition range where the spinodal

decomposition can take place, the separation kinetics looks like the nucleation process, as shown in Fig. 3; the system needs an incubation period to start the phase separation so as to reduce the elastic strain energy. Also for charge, it has been proven that the phase separation kinetics is significantly retarded due to the elastic effect; see Fig. 5. This simulation result is in good agreement with the experimental facts that the phase separation kinetics are significantly suppressed or retarded,[7–9] and this can be easily understood by the fact that the nucleation is fundamentally difficult to occur in this system. From the simulation results with various charge rates, at all the rates the phase-separation-onset composition was significantly higher than the spinodal point (the cross point of the spinodal line and temperature) determined by the free-energy function.

4. The stability of the anisotropic interfaces were considered here; the *bc* interface is considerably stable but the *ab* interface is quite unstable in terms of the elastic strain energy (this is also the case for the *ac* interface, but not presented here). This is because the coherent strain along the *a* axis is the largest and the formation of the *bc* interface is free from the coherent connection associated with the *a* axis. Therefore, when the phase separation occurs, the system cannot produce the *ab* interface and also *ac* interface. These are consistent with the actual microstructures observed in a transmission electron microscope (TEM).[29, 32, 33] Thus, in terms of the elastically stable interfaces, it can be concluded that the usual core-shell model is not plausible, as the other interfaces (except for the *bc* interface) are unstable in terms of the coherent strain energy.

5. The present simulation shows that the domino-cascade mode is also possible if the nucleation can take place (possibly around the particle surface). However, also in such a case, the spinodal mode can also take place in the far distant regions from the initial nucleus. Namely, in a single particle, it is reasonable to consider that the phase separation proceeds via the mixture mode of domino cascade and spinodal decomposition. This result obtained from the computer simulation is in consistent with the recent experimental observation.[25]

Acknowledgements

This work was partly supported by Advanced Low Carbon Technology Research and Development Program (ALCA) and a Grant-in-Aid from Special Coordination Funds for Promoting Science and Technology commissioned by JST, MEXT of Japan. This work was also partly supported by the New Energy and Industrial Technology Development Organization (NEDO) under the Research and Development Initiative for Scientific Innovation of New Generation Batteries (RISING).

[1] A. K. Padhi, K. S. Nanjundaswamym, & J. B. Goodenough, J. Electrochem. Soc. **144**, 1188-1194 (1997).
[2] A. Yamada, H. Koizumi, S. Nishimura, N. Sonoyama, R. Kanno, M. Yonemura, T. Nakamura, & Y. Kobayashi, Nature Mater. **5**, 357-360 (2006).
[3] N. Meethong, H.-Y. S. Huang, W. C. Carter, and Y.-M. Chiang, Electrochem. Solid-State Letters **10**, A134-A138 (2007).
[4] G. Kobayashi, S. Nishimura, M.-S. Park, R. Kanno, M. Yashima, T. Ida, and A. Yamada, Adv. Funct. Mater. **19**, 395-403 (2009).
[5] N. Meethong, H.-Y. S. Huang, S. A. Speakman, W. C. Carter, and Y.-M. Chiang, Adv. Funct. Mater. **17**, 1115-1123 (2007).
[6] P. Gibot, M. Casas-Cabanas, L. Laffont, S. Levasseur, P. Carlach, S. Hamelet, J.-M. Tarascon, and C. Masquelier, Nature Mater. **7**, 741-747 (2008).
[7] H. -H. Chang, C. -C. Chang, H. -C. Wu, M. -H. Yang, H. -S. Sheu, and N. -L. Wu, Electrochem. Commun. **10**, 335-339 (2008).
[8] J. B. Leriche, S. Hamelet, J. Shu, M. Morcrette, C. Masquelier, G. Ouvrard, M. Zerrouki, P. Soudan, S. Belin, E. Elkaïm, and F. Baudelet, J. Electrochem. Soc. **157**, A606-A610 (2010).
[9] X. J. Wang, C. Jaye, K. -W. Nam, B. Zhang, H. -Y. Chen, J. Bai, H. Li, X. Huang, D. A. Fischer, and X. -Q. Yang, J. Mater. Chem. **21**, 11406-11411 (2011).
[10] M. Wagemaker, F. M. Mulder, and A. Van der Ven, Adv. Mater. **21**, 2703-2709 (2009).
[11] D. A. Cogswell, and M. Z. Bazant, ACS Nano **6**, 2215-2225 (2012).
[12] K. Hirai, T. Ichitsubo, T. Uda, A. Miyazaki, S. Yagi, and E. Matsubara, Acta Mater. **56**, 1539-1545 (2008).
[13] T. Ichitsubo, S. Yukitani, K. Hirai, S. Yagi, T. Uda, E. Matsubara, J. Mater. Chem. **21**, 2701-2708 (2011).
[14] A. G. Khachaturyan, Theory of Structural Transformation in Solids, (Wiley, New York, 1983).
[15] L. Q. Chen, Y. Wang, and A. G. Khachaturyan, Philos. Mag. Lett. **65**, 15 (1992).
[16] T. Ichitsubo, K. Tanaka, M. Koiwa, and Y. Yamazaki, Phys. Rev. B **62**, 5435 (2000).
[17] M. Tang, H.-Y. Huang, N. Meethong, Y.-H. Kao, W. C. Carter, and Y.-M. Chiang, Chem. Mater. **21**, 1557-1571 (2009).
[18] M. Tang, J. F. Belak, and M. R. Dorr, J. Phys. Chem. C **115**, 4922-4926 (2011).
[19] P. Bai, D. A. Cogswell, and M. Z. Bazant, Nano Lett. **11**, 4890-4896 (2011).
[20] J. D. Eshelby, Proc. R. Soc. **A 241**, 376-396 (1957).
[21] T. Mura, Micromechanics of Defects in Solids, 2nd ed, revised (Martinus Nijhoff Pul, The Hegue, 1987).
[22] J.W. Cahn, & J. E. Hilliard, J. Chem. Phys. **28**, 258-267 (1958).
[23] J. W. Cahn, Acta. Metall. **9**, 795-801 (1961).
[24] J. W. Cahn, Acta. Metall. **10**, 179-183 (1962).
[25] G. Brunetti, D. Robert, P. Bayle-Guillemaud, J. L. Rouvière, E. F. Rauch, J. F. Martin, J. F. Colin, F. Bertin, and C. Cayron, Chem. Mater. **23**, 4515-4524 (2011).
[26] T. Ichitsubo, T. Doi, E. Matsubara, Y. Yamada, K. Chihara, T. Kida, K. Tokuda, S. Yagi, S. Okada, J. Yamaki, in preparation.
[27] R. Malik, F. Zhou, and G. Ceder, Nat. Mater. **10**, 587-590 (2011).
[28] W. Dreyer, J. Jamnik, C. Guhlke, R. Huth, J. Moškon, and M. Gaberšcek, Nature Mater. **9**,

448-453 (2010).
[29] C. V. Ramana, A. Mauger, F. Gendron, C. M. Julien, and K. Zaghib, J. Power Sources **187**, 555-564 (2009).
[30] T. Maxisch, and G. Ceder, Phys. Rev. B **73**, 174112 (2006).
[31] D. Morgan, A. Van der Ven, and G. Ceder, Electrochem. Solid-State Lett. **7**, A30-A32 (2004).
[32] G. Chen, X. Song, and T. J. Richardson, Electrochem. Solid-State Lett. **9**, A295-A298 (2006).
[33] L. Laffont, C. Delacourt, P. Gibot, M. Y. Wu, P. Kooyman, C. Masquelier, and J. M. Tarascon, Chem. Mater. **18**, 5520-5529 (2006).
[34] C. Delmas, M. Maccario, L. Croguennec, F. Le. Cras, and F. Weill, Nature Mater. **7**, 665-671 (2008).
[35] K. T. Lee, W. H. Kan, and L.F. Nazar, J. Am. Chem. Soc., **131**, 6044-6045 (2009).

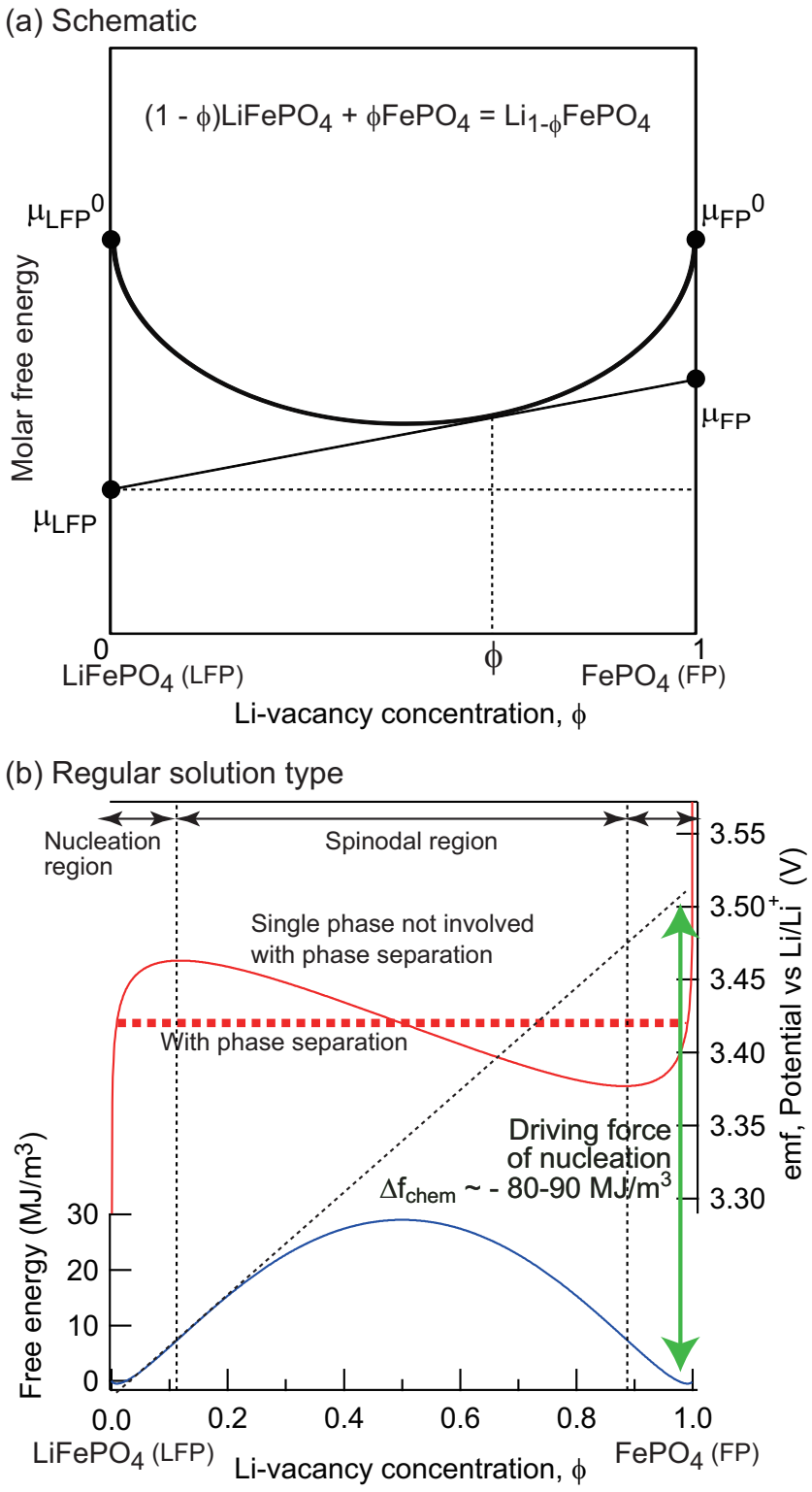

FIG. 1: (a) Schematic illustration of molar free-energy function with regard to the Li-vacancy composition for explaining the chemical potential of Li atoms in the ionic solid. (b) The free-energy function of regular solution type with $\Omega = 12$ kJ/mol (bottom) and the chemical potential of Li atoms (upper) for the pseudo-binary $LiFePO_4/FePO_4$ system.

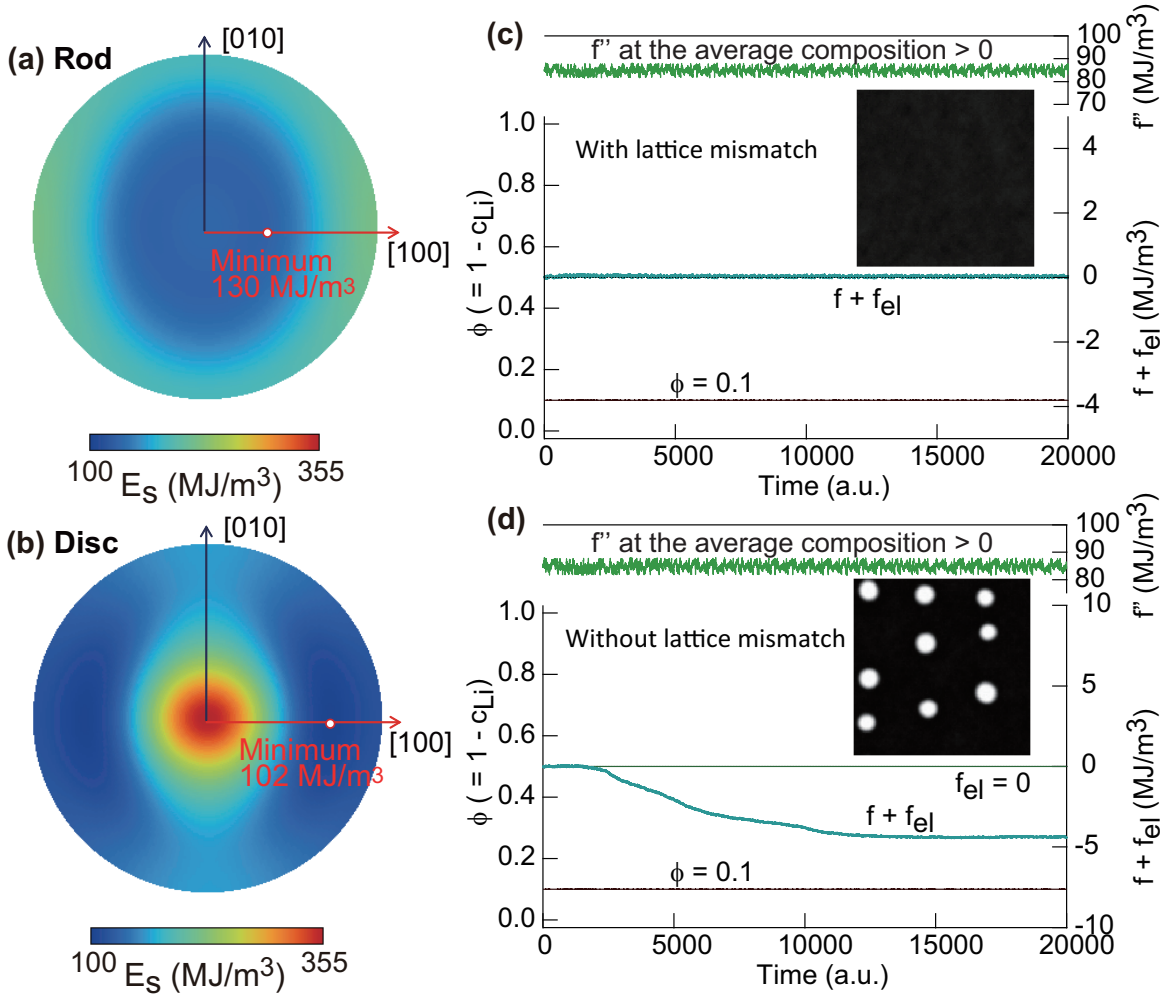

FIG. 2: The left figures show the [001] pole figures for the elastic strain energy E_s calculated for typical shapes of $FePO_4$ nucleus formed in a infinite $LiFePO_4$ matrix: (a) rod shape, and (b) disc (plate) shape. The minimum strain energy (102 MJ/m^3) is realized for the disc shape when the disc normal direction is almost [101] or [100] directions. The strain energy for a sphere precipitate is calculated to be about 160 MJ/m^3. The right figures show the kinetics of the nucleation processes by the phase-field simulations; (c) with and (d) without the coherent strain due to the lattice mismatch. In this simulation, the standard deviation of $\int_t^{t+\Delta t} \theta dt'$ is arbitrarily set at 0.005 as the thermal fluctuation.

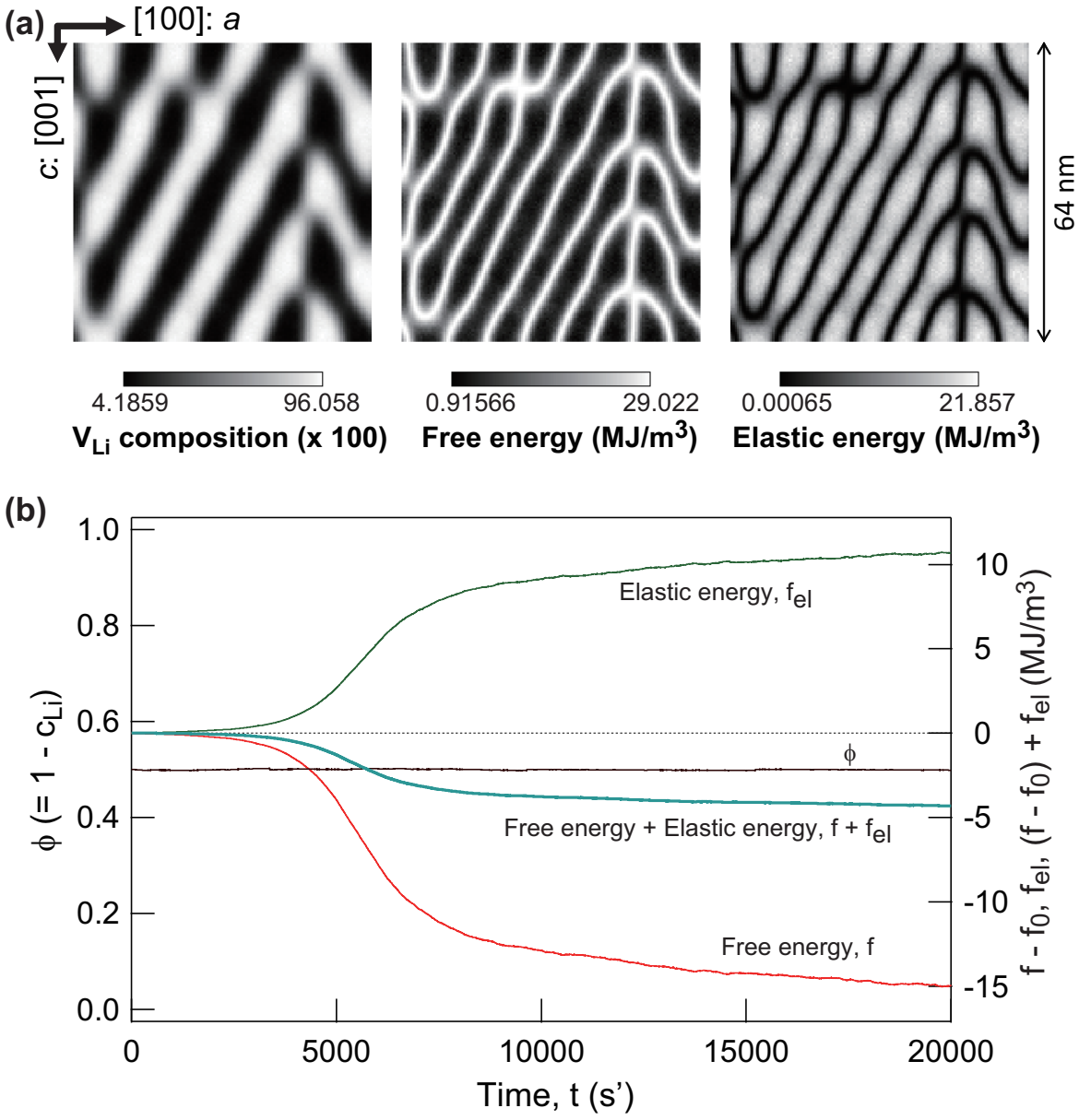

FIG. 3: (a) Simulated microstructure (black; $LiFePO_4$, white: $FePO_4$) after spinodal decomposition at a constant $\phi = 0.5$ at $t = 20000$ s' (upper): (left) Li composition, (middle) free energy, (right) elastic strain energy. (b) Thermodynamic quantities accompanied by the spinodal decomposition with the coherent lattice mismatch. In this simulation, the value of gradient energy coefficient K_S corresponding to $\gamma_S \approx 40$ mJ/m^2 was used.

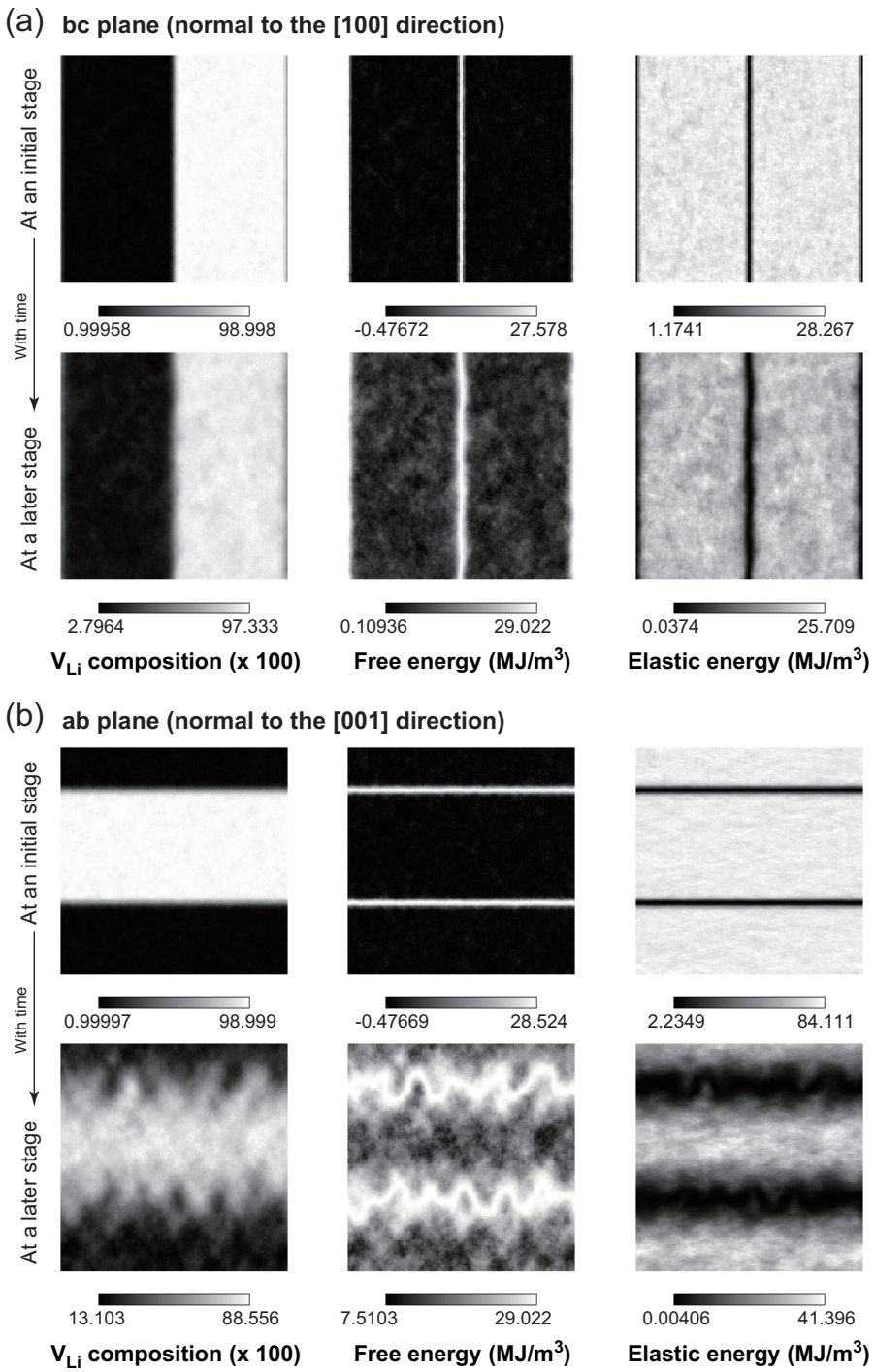

FIG. 4: The stability of the anisotropic interfaces: (a) bc plane and (b) ab plane. In the simulation, the gradient energy K_{s} corresponding to $\gamma_{\mathrm{S}} = 40$ mJ/m^2 is used.

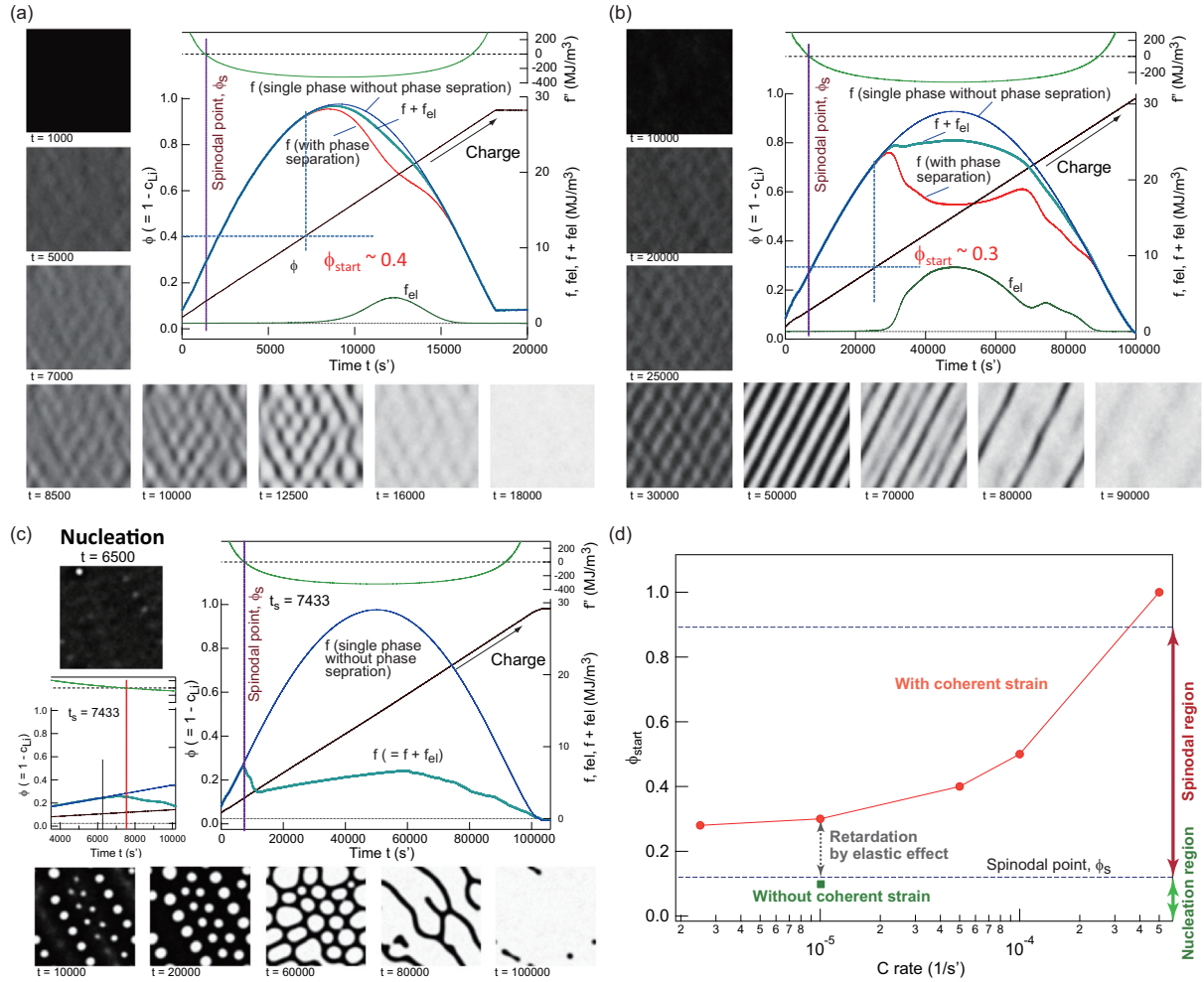

FIG. 5: Simulated microstructure evolution (black; $LiFePO_4$, white: $FePO_4$) and various energies obtained during charge process in $LiFePO_4$; (a) C rate $\approx 1/(20000$ s'), (b) C rate $\approx 1/(100000$ s') with the coherent strain, and (c) C rate $\approx 1/(100000$ s') without the coherent strain. (d) The onset composition where the phase separation starts to occur as a function of the C rate. The simulation started from the homogeneous $LiFePO_4$ matrix to observe nucleation and spinodal processes. As is expected, no nucleation is detected in the coherent case, and even spinodal decomposition occurs in a very later stage after reaching the spinodal point (ϕ_s).

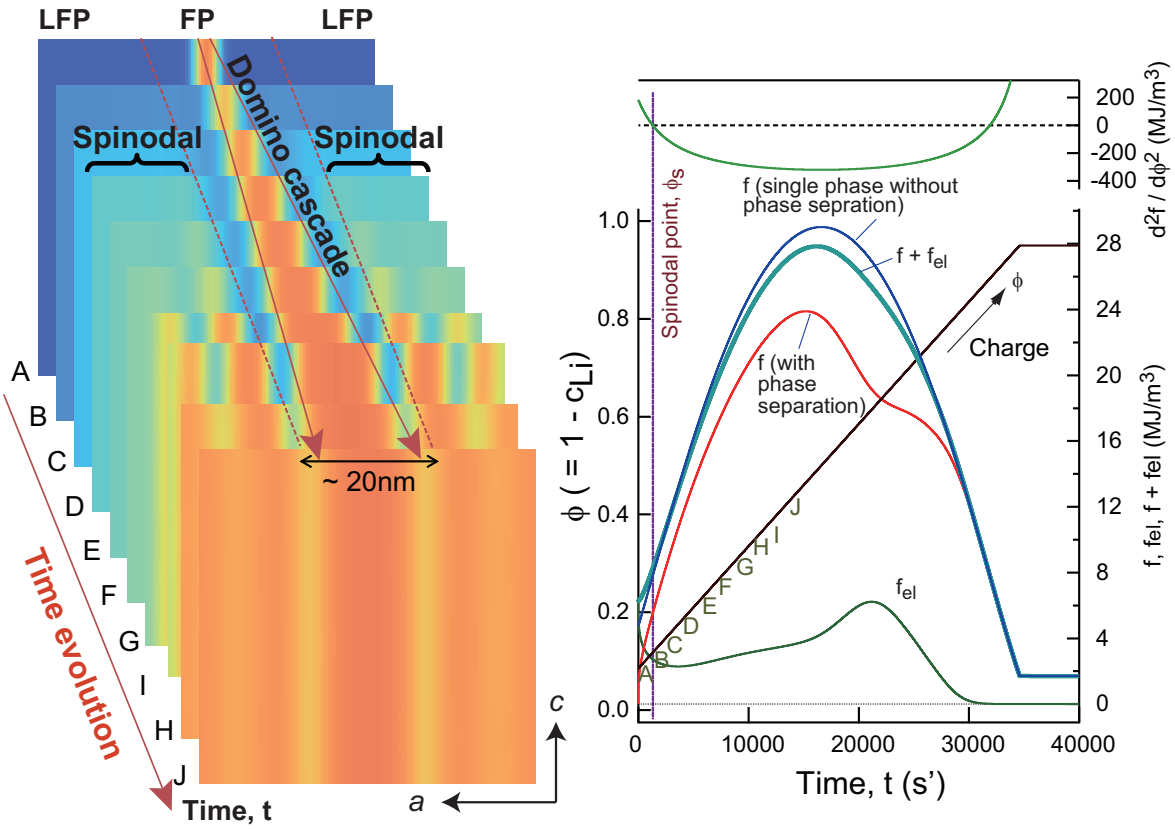

FIG. 6: Mixture mode of domino cascade and spinodal decomposition during charge process [blue; $LiFePO_4$ (LFP), orange: $FePO_4$ (FP)] (left) and time dependence of the free energy, elastic energy, and sum of these energies during charge process (right). In the simulation, the $FePO_4$ plate with the (100) coherent interface is set precedently. The domino cascade mode is observed in the early stage within the range of about 20 nm, and followed by the spinodal decomposition in the regions distant from the initial plate.